Journal of Materials Chemistry A

ROYAL SOCIETY OF CHEMISTRY

PAPER

View Article Online
View Journal | View Issue



Cite this: J. Mater. Chem. A, 2020, 8, 11545

# Multiple diffusion pathways in $Li_xNi_{0.77}Co_{0.14}Al_{0.09}O_2$ (NCA) Li-ion battery cathodes†

Thomas E. Ashton, *[a] Peter J. Baker, [b] Dustin Bauer,[a] Alexandra R. Groves, [a] Carlos Sotelo-Vazquez, [a] Takashi Kamiyama,[c] Takeshi Matsukawa, [d] Kenji M. Kojima[ef] and Jawwad A. Darr[a]

Received 7th April 2020
Accepted 16th May 2020

DOI: 10.1039/d0ta03809a

rsc.li/materials-a

Experimental evidence for the presence of two computationally theorised diffusion pathways, namely the oxygen dumbbell hop (ODH) and tetrahedral site hop (TSH), has been given for the first time by muon spin relaxation (μSR) on sub-stoichiometric $Li_xNi_{0.77}Co_{0.14}Al_{0.09}O_2$. μSR has proven to be a powerful tool that is able to discriminate between diffusion pathways that occur on different timescales on a local level, where bulk electrochemical techniques cannot. Whereas the estimated values of $D_{Li}$ at lithium concentrations of 0.87 and 0.71 were found to be on the order of $10^{-11}$ by electrochemical impedance spectroscopy, contributions to diffusion from ODH and TSH were determined to be on the order of $10^{-11}$ and $10^{-10}$ $cm^2$ $s^{-1}$, and a factor of four decrease in $E_a$ for both samples, in excellent agreement with theoretical calculations on related compounds. Rietveld refinement of both X-ray and neutron diffraction data was also used to interrogate the local structure of the materials where no contribution from $Li^+/Ni^{2+}$ cation mixing was observed.



## Introduction

As the global energy demand continues to rise, increased effort is directed towards the efficient harvesting (particularly from renewables), utilisation and storage of electrical energy to meet the needs of an increasingly urbanised global population and to alleviate the effects of climate change.[1,2] Towards the latter goal, the electrification of transport to move away from fossil fuels and linking this to smart charging grids will need development. Commercial rechargeable Lithium Ion Batteries (LIBs) with high energy densities are thus of interest in this regard,[3] most notably those with $LiCoO_2$ type layered metal oxide cathodes.[4,5] Such layered materials can be doped to improve performance characteristics, *e.g.* rate capability, operating voltage and structural/thermal stability.

Recently, layered, nickel rich $LiNi_{1-x}M_xO_2$ materials have been developed as inexpensive and more sustainable high-energy cathodes for secondary Li ion batteries (where $x \geq 0.2$ and M is a substituent transition metal or combination of metals). Pure $LiNiO_2$ has shown poor performance as a cathode due to anti-site defects, where $Ni^{2+}$ species locate in Li 3a sites in the crystal structure and hamper $Li^+$ diffusion.[6] Improvement in performance was shown by substituting up to 20 at% Ni for Co, reducing the $Li^+/Ni^{2+}$ cationic disorder and reducing oxygen loss at high states-of-charge and improving safety.[7] Further stabilisation strategies include the co-substitution of nickel with cobalt and another third element to form a ternary lithium containing metal oxide ($LiNi_xCo_yM_zO_2$, where $x + y + z = 1$). Where M = Mn, this is known as the widely researched "NMC" family of materials.

Specifically, Al substituted materials such as $LiNi_{0.80}Co_{0.15}Al_{0.05}O_2$ (NCA) are of increasing of interest for commercial battery applications due to its stable operating voltage of 3.8 V *versus* $Li/Li^+$ and observed gravimetric capacity between 175 and 200 mA h $g^{-1}$.[8] Inclusion of Al in the host structure leads to higher thermal stability and increased electrochemical properties.[9–14] Although the macroscopic electrochemical behaviour of NCA has been scrutinised in detail, the fundamental processes governing the operation of these materials is not well understood. Arguably, the most important of these processes remains the diffusion of lithium through the host insertion electrode, as lithium diffusion is ultimately responsible for cell operation. Many complementary techniques

[a]Department of Chemistry, University College London, 20 Gordon Street, Bloomsbury, London, WC1H 0AJ, UK. E-mail: t.ashton@ucl.ac.uk
[b]ISIS Pulsed Neutron and Muon Source, STFC Rutherford Appleton Laboratory, Harwell Science and Innovation Campus, Didcot, Oxfordshire, OX11 0QX, UK
[c]Materials & Life Science Division, J-PARC Center, Tokai, Ibaraki 319-1195, Japan
[d]Frontier Research Center for Applied Atomic Sciences, Ibaraki University, 162-1, Shirakata, Tokai, Ibaraki 319-1106, Japan
[e]Centre for Molecular and Materials Science, TRIUMF, 4004 Wesbrook Mall, Vancouver, B.C., V6T 2A3, Canada
[f]Stewart Blusson Quantum Matter Institute, University of British Columbia, 2355 East Mall, Vancouver, B.C., V6T 1Z4, Canada

† Electronic supplementary information (ESI) available. See DOI: 10.1039/d0ta03809a

have been used to probe the diffusion mechanics; electrochemical (cyclic voltammetry,[15] titration techniques[16–18] and impedance spectroscopy[19]), physical (nuclear magnetic resonance[20] and muon spin relaxation[21–23]) and computational methods,[24–26] each with their own associated benefits and limitations.

Muon spin relaxation (μSR) has previously been employed to investigate $Li^+$ diffusion in many LIB materials including cathodes and solid-state electrolytes.[21–23,27–31] As μSR is a local probe technique, atomic scale diffusion can be probed as a local average within the material. This allows the measurement of diffusion processes independent from contributions to diffusion encountered in bulk measurements, for instance intercalation-based processes arising from grain boundary and/or surface interactions. The cathode materials that have been investigated to date include sub-stoichiometric $Li_xCoO_2$ and $LiNi_{\frac{1}{3}}Mn_{\frac{1}{3}}Co_{\frac{1}{3}}O_2$ (NMC-111).[29,32] Values for the lithium diffusion rate ($D_{Li}$) determined by μSR in $Li_{0.73}CoO_2$ and $Li_{0.53}CoO_2$ of $7(\pm2) \times 10^{-10}$ and $2.5(\pm0.8) \times 10^{-10}$ $cm^2\ s^{-1}$, respectively, were comparable to values calculated from first principles.[24] However, these first principles calculations suggested that decreasing lithium concentration could also promote a second $Li^+$ diffusion pathway (which has not been observed experimentally, to date). In these materials only one contribution to $Li^+$ diffusion was shown and assumed a single mechanism with an activation energy $\approx$ 100 meV.[33] In comparison, previous bulk electrochemical studies using GITT on commercial NCA shows a $D_{Li}$ of $10^{-10}$ cm $s^{-1}$ and activation energies $\approx$ 260 eV.[34] It is important to note that computational calculations and experimental methods have regularly overestimated $E_a$ of $Li^+$ diffusion when compared to local μSR measurements.[21,23] All of these studies have been based on a single contribution to $Li^+$ diffusion, however computational investigations on the parent material $LiCoO_2$ suggest two possible diffusion routes, namely the Oxygen Dumbbell Hop (ODH) and Tetrahedral Site Hop (TSH).[24] A representation of the two mechanisms can be seen in Fig. 1(a).

The ODH mechanism proceeds when a lithium migrates into an isolated vacancy (red circle), where the minimum energy path requires a lithium ion to pass between a dumbbell of two oxygen ions. Alternatively, the TSH mechanism occurs if the lithium ion can hop into a site that is part of a divacancy by passing through the tetrahedral site between the original position and the two vacant sites. The same mechanisms have also been calculated *in silico* to occur in $Li_xNi_{0.5}Mn_{0.3}Co_{0.2}O_2$, and suggest that metal site substitution of Co for other metals (such as Mn and Ni) can lead to a lowering of the activation energy of diffusion (120 meV) *versus* the analogous $LiCoO_2$ (210 meV).[35,36] The decrease in activation energy has been rationalised by two contributions: (i) weaker repulsive $Li^+$–$Ni^{2+}$ interactions compared to $Li^+$–$Co^{3+}$; (ii) a larger *c* lattice parameter. The relationship between the $E_a$ calculated for ODH and TSH consistently adhere to $E_a^{TSH} \approx \frac{1}{4} \times E_a^{OSH}$.

Herein, the lithium diffusion mechanics in lithium deficient NCA were investigated by bulk electrochemical impedance spectroscopy (EIS) and local μSR measurements. The μSR behaviour has provided the first experimental evidence for the presence of two distinct lithium diffusion mechanisms in NCA cathode materials.

## Results and discussion

### Structural characterisation

Sub-stoichiometric $Li_nNi_xCo_yAl_zO_2$ particles were prepared by solid-state synthesis, described in the Experimental section. The syntheses yielded fine black powders which were characterised by Powder X-ray Diffraction (PXRD). The crystal structures of the NCA materials were analysed by subsequent Rietveld refinement of the PXRD data shown in Fig. 2. A single rhombohedral phase, typical of $LiCoO_2$-type layered materials (space group: $R\bar{3}m$), was observed in both cases and showed good agreement with the expected profile from an NCA reference pattern (ICSD no. 257247).[37] Lattice parameter values showed <0.5% difference compared to the reference structure ($\Delta_{ref}$): $a = 2.8739$ Å ($\Delta_{ref} = 0.0071$), $b = 2.8739$ Å ($\Delta_{ref} = 0.0071$) and $c = 14.1937$ Å ($\Delta_{ref} = 0.0031$) for $Li_{0.87}$NCA, and $a = 2.8712$ Å ($\Delta_{ref} = 0.0071$), $b = 2.8712$ Å ($\Delta_{ref} = 0.0071$) and $c = 14.1902$ Å ($\Delta_{ref} = -0.0003$) for $Li_{0.71}$NCA. The transition metal stoichiometry of both samples was found to be $Li_nNi_{0.77}Co_{0.14}Al_{0.09}O_2$ using X-ray Fluorescence Spectroscopy (XRF).

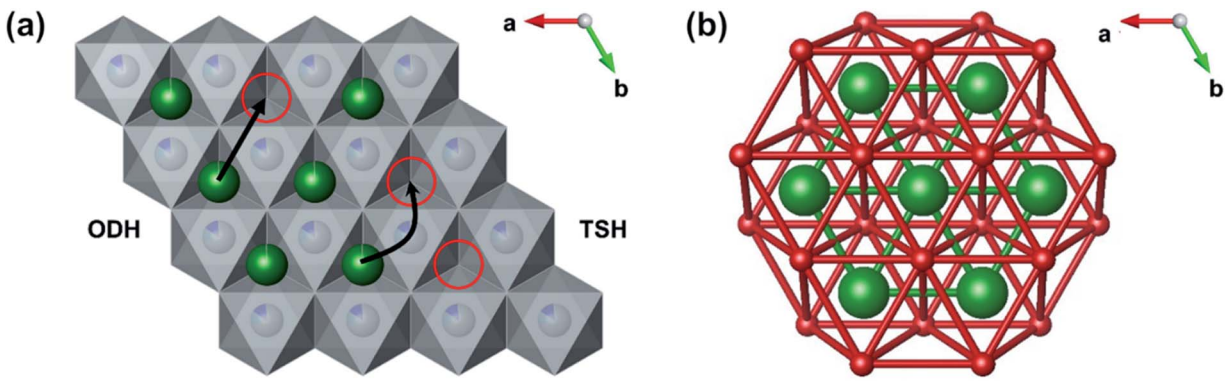


Fig. 1 (a) Diagram showing the octahedral dumbbell hop (ODH) and tetrahedral site hop (TSH) mechanisms in $LiCoO_2$, with Li atoms (green), $MO_6$ polyhedra (grey) and vacancies (red). (b) Diagram showing all possible oxygen dumbbells (red) and their interaction with the ODH lithium diffusion paths (green) in the $LiO_6$ slab.

 

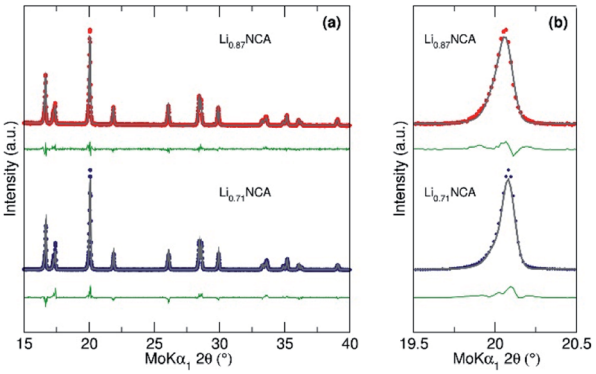


Fig. 2 (a) Rietveld refinement of Powder X-ray Diffraction (PXRD) patterns collected for $Li_{0.87}NCA$ (red) and $Li_{0.71}NCA$ (blue) showing single phase rhombohedral $R\bar{3}m$ (ICSD no. 257247). Lattice parameters and refinement values can be found in the ESI (Table 1†). (b) Zoomed area of the PXRD data in (a) between 19.5 and 20.5° $2\theta$ showing the fit to the (104) reflection.

$Li^+/Ni^{2+}$ cation mixing is a prevalent cause in disrupting $Li^+$ diffusion in layered transition metal oxides and was thus investigated by Neutron Powder Diffraction (NPD) and subsequent Rietveld refinement, for both samples. Firstly, the fits were constrained to adhere to $(Li_{\gamma-\delta}Ni_{\delta})_{3b}(Li_{\delta}Ni_{0.77}Co_{0.14}Al_{0.09})_{3a}O_2$ (Table 1); $g$ is the occupancy of the atoms, $\gamma$ is the estimated $Li^+$ concentration from NPD and $\delta$ is the measure of atoms participating in cation mixing and $B$ is the Debye–Waller factor (attenuation of neutron radiation by thermally induced motion of the atoms). The metals composition was fixed at the values obtained from XRF for each sample.

During the initial fitting, the model could not converge with a positive value of $\delta$ for either sample suggesting no detectable $Li^+/Ni^{2+}$ cation mixing was present in either sample. Fixing $\delta$ to 0 allowed the model to converge and a good fit to lattice parameters taken from a rhombohedral $R\bar{3}m$ (ICSD no. 257247) reference structure was obtained (Fig. 3) for both $Li_{0.87}NCA$ ($R_{wp}$ = 2.66, $R_e$ = 0.564, $R_F$ = 2.58) and $Li_{0.71}NCA$ ($R_{wp}$ = 3.09, $R_e$ = 0.624, $R_F$ = 2.79). The $Li^+$ concentration in each sample was estimated to be $Li_{0.87}NCA$ $\gamma$ = 0.8704(11) and $Li_{0.71}NCA$ $\gamma$ = 0.7080(12). A full table of calculated parameters can be found in the ESI.†

The $Li^+$ concentration was fixed at the determined values for each sample and further fitting was carried out to estimate the lattice parameters, summarized in Table 2 with the PXRD values for comparison. The calculated lattice volumes marginally decreased by <0.1% with decreasing $Li^+$ content, in good agreement with previous crystallographic studies of NCA and NMC based materials.[38–41] No significant difference in Li–Li distance was observed between $Li_{0.87}NCA$ ($\Delta_{ref}$ = 0.0055 Å) and $Li_{0.71}NCA$ ($\Delta_{ref}$ = 0.0048 Å) and was thus not expected to significantly contribute to any difference in $Li^+$ diffusion kinetics.

Table 1 Rietveld parameters applied for the fitting of NPD data collected for $Li_{0.87}NCA$ and $Li_{0.71}NCA$

| Atom | Site | $g$ | $x$ | $y$ | $z$ | $B$(iso) |
|---|---|---|---|---|---|---|
| Li1 | 3b | $\gamma-\delta$ | 0 | 0 | $\frac{1}{2}$ | ≈1 |
| Ni1 | 3b | $\delta$ | 0 | 0 | $\frac{1}{2}$ | $B$(Li1) |
| Ni2 | 3a | $0.77-\delta$ | 0 | 0 | 0 | ≈0.3 |
| Co2 | 3a | 0.14 | 0 | 0 | 0 | $B$(Ni2) |
| Al2 | 3a | 0.09 | 0 | 0 | 0 | $B$(Ni2) |
| Li2 | 3a | $\delta$ | 0 | 0 | 0 | $B$(Ni2) |
| O1 | 6c | 1 | 0 | 0 | ≈0.259 | ≈1 |

The particle sizes of $Li_{0.87}NCA$ and $Li_{0.71}NCA$ were investigated further by scanning electron microscopy (SEM), seen in Fig. 4(a) and (b) respectively. The average particle size was calculated to be 3.4 μm ($\sigma$ = 0.32 μm) for $Li_{0.87}NCA$, while a bimodal distribution was observed for $Li_{0.71}NCA$ corresponding to average particle sizes of 2.4 μm ($\sigma$ = 0.65 μm) and 0.73 μm ($\sigma$ = 0.12 μm) for $Li_{0.71}NCA$.

## Bulk diffusion in $Li_xNCA$ (electrochemical characterisation)

Electrochemical impedance spectroscopy (EIS) was employed to investigate the bulk lithium diffusion in the lithium deficient NCA samples. Fig. 5(a) shows Nyquist plots (real *versus* imaginary impedance) for $Li_{0.87}NCA$ and $Li_{0.71}NCA$ before and after electrochemical cycling at a C/20 rate for 20 cycles. After cycling, both samples showed one semi-circle due to charge transfer resistance ($R_{ct}$) at the electrode surface, followed by a tail due to resistance from ionic transport (Warburg impedance).[42] After cycling, a second impedance contribution appeared due to the formation of a solid-electrolyte interphase ($R_{SEI}$) on the NCA particles, as described in previous reports on layered Li-ion cathodes.[43] $R_{ct}$ values of 51 and 59 Ω were extracted for $Li_{0.87}NCA$ and $Li_{0.71}NCA$, respectively, by fitting a modified Randles cell model (see ESI†) to the data before electrochemical cycling.[44] These $R_{ct}$ values were largely preserved after cycling and the additional $R_{SEI}$ contributions were calculated as 51 and 54 Ω for $Li_{0.87}NCA$ and $Li_{0.71}NCA$, respectively.

Fig. 5(b) shows the Warburg plot for the two samples, where the gradient of the line is equal to the Warburg coefficient for the material ($\sigma_w$). $D_{Li}$ for $Li_{0.87}NCA$ and $Li_{0.71}NCA$ were subsequently estimated using eqn (1), where: $R$ is the gas constant, $T$ is the temperature (298 K), $A$ is the electrode area, $F$ is the Faraday constant and $C$ is the concentration of charge carriers.

$$D_{Li} = 0.5\left(\frac{RT}{AF^2\sigma_w C}\right)^2 \quad (1)$$

Values of $D_{Li}$ were estimated as $3 \times 10^{-11}$ $cm^2$ $s^{-1}$ for $Li_{0.87}NCA$ and $1 \times 10^{-11}$ $cm^2$ $s^{-1}$ $Li_{0.71}NCA$, in excellent agreement with previous EIS studies on NCA at similar $Li^+$ concentrations ($D_{Li} = 4 \times 10^{-11}$ for $[Li^+] = 0.75$).[19]

## Local diffusion in $Li_xNCA$ (μSR)

To investigate the diffusion mechanics on a local scale, μSR measurements were made from 150 to 400 K at 10 K intervals. At each temperature, three measurements were made at longitudinal magnetic field strengths ($B_{LF}$) of 0 (zero-field), 5 and 10 G to sequentially decouple the muon relaxation from nuclear magnetic fields within the samples (Fig. 6(a)). As $B_{LF}$ increases,

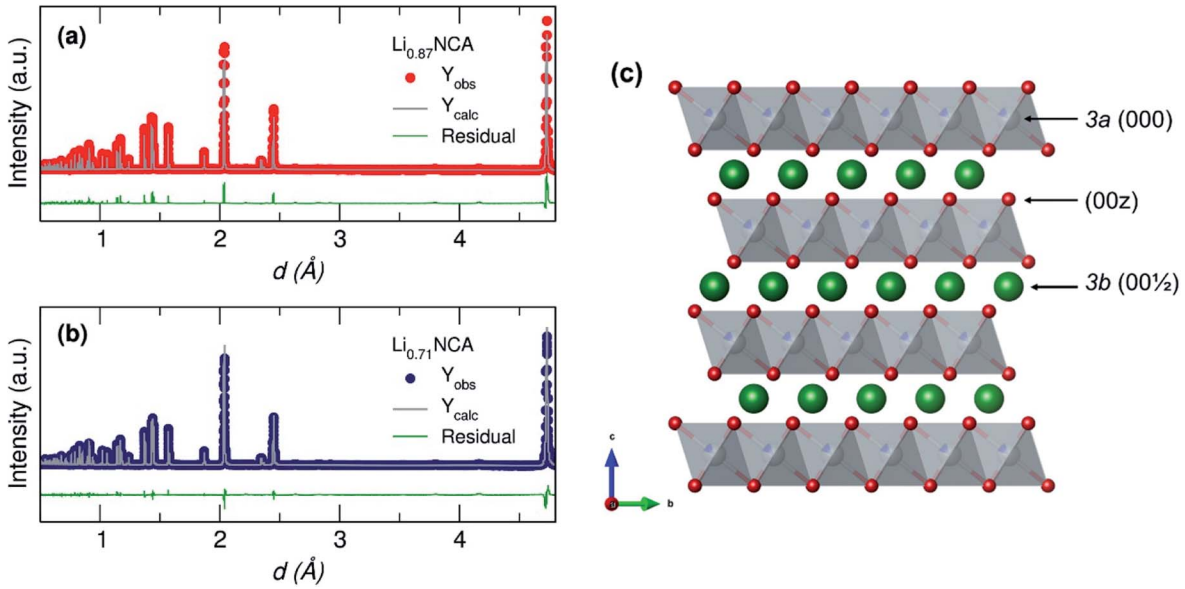


Fig. 3 Rietveld refinement of NPD collected for (a) $Li_{0.87}$NCA and (b) $Li_{0.71}$NCA showing a good fit in both cases to the model described in Table 1 based on standard data for NCA (space group $R\bar{3}m$; ICSD coll. code: 257247). (c) Crystal structure of NCA showing the three main crystallographic sites of interest (000, 00*z* and 001/2) where Li atoms are green, $MO_6$ polyhedra are grey and O atoms are red.

Table 2 Lattice parameters, cell volume and Li–Li distance calculated from PXRD and NPD. The neutron refinement data has also been given in full, with errors in the ESI, Table S1a and b

| | NPD | | | | | PXRD | | | | |
|---|---|---|---|---|---|---|---|---|---|---|
| | *a* (Å) | *b* (Å) | *c* (Å) | *V* (Å$^3$) | Li–Li (Å) | *a* (Å) | *b* (Å) | *c* (Å) | *V* (Å$^3$) | Li–Li (Å) |
| $Li_{0.87}$NCA | 2.8697 | 2.8697 | 14.1878 | 101.1867 | 2.8697 | 2.8739 | 2.8739 | 14.1937 | 101.5242 | 2.8739 |
| $Li_{0.71}$NCA | 2.8689 | 2.8689 | 14.1829 | 101.0935 | 2.8689 | 2.8712 | 2.8712 | 14.1902 | 101.3085 | 2.8712 |

there is a decrease in the relaxation of the muon decay asymmetry suggesting that the decoupling was effective at the magnitude of applied fields chosen. At all values of $B_{LF}$ the slow relaxation of the data is indicative of the diffusion mediated perturbation of muon spin polarization from $^6$Li and $^7$Li.[21]

Data from all three fields at a given temperature were fit simultaneously to a modified Kubo–Toyabe relaxation model to describe the dynamic diffusion processes multiplied by a Gaussian relaxation function to account for temperature independent fluctuations in $Li^+$ diffusion, and a constant background component.[45] Fig. 6(b) shows the extracted values

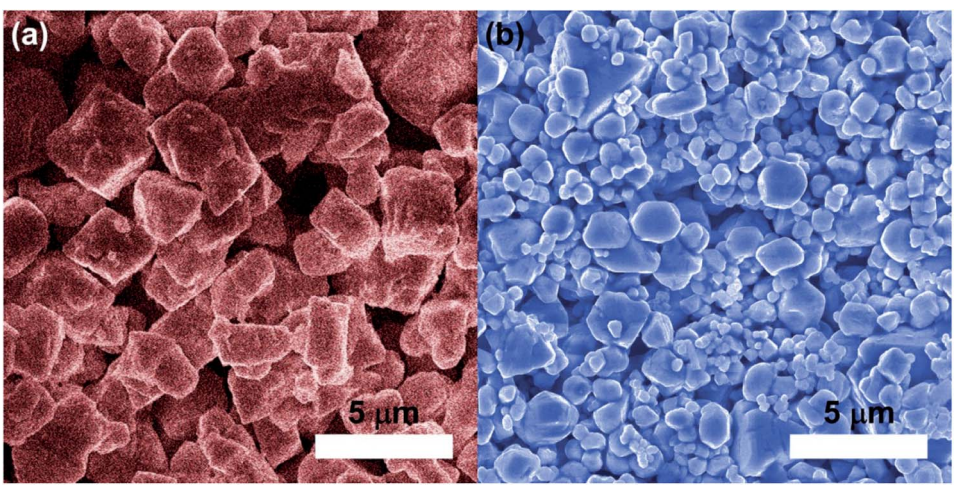


Fig. 4 Scanning electron micrographs of (a) $Li_{0.87}$NCA and (b) $Li_{0.71}$NCA.

 

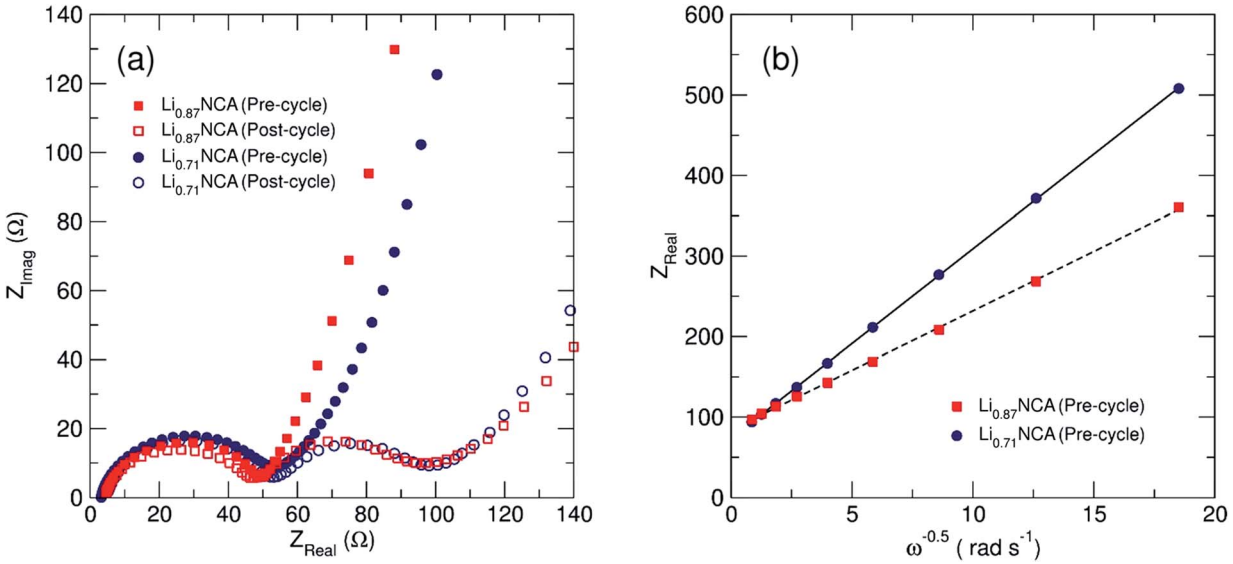


Fig. 5 Electrochemical impedance spectroscopy (EIS) results for $Li_{0.87}NCA$ and $Li_{0.71}NCA$. (a) The Nyquist plot pre- and post-cycling, showing the evolution of a second resistance contribution, and (b) the Warburg plot used to calculate $D_{Li}$ of $Li_{0.87}NCA$ and $Li_{0.71}NCA$.

for the local field distribution width ($\Delta$). A gentle decrease in $\Delta$ was observed due to the motional narrowing of the magnetic environment the muon experiences, similarly observed in other μSR diffusion experiments. Importantly no unexpected magnetic behaviour that would affect the calculated values of the muon relaxation fluctuation rate ($\nu$) which can be seen in Fig. 7(a), were observed.

Both $Li_{0.87}NCA$ and $Li_{0.71}NCA$ display two contributions to the fluctuation rate in the low $T$ range (160 to 260 K) and high $T$ range (340 to 380 K). Although these observations cannot be explicitly assigned to their particular processes by μSR alone, two energy barriers have been predicted by the previously discussed theoretical work: a more rapid TSH mechanism and a less rapid ODH mechanism.[24] Therefore, the lower $T$ contribution was assigned to $D_{Li}^{TSH}$ and higher $T$ to $D_{Li}^{ODH}$.

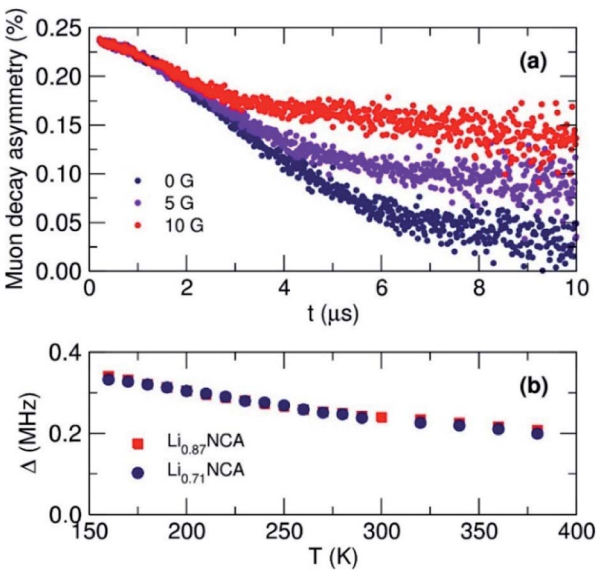


Fig. 6 (a) Raw muon asymmetry data collected at 300 K for $Li_{0.87}NCA$ with an applied longitudinal field of 0, 5 and 10 G. (b) The estimated values for the field distribution width ($\Delta$) as a function of temperature for $Li_{0.87}NCA$ and $Li_{0.71}NCA$.

As temperature increases the thermal equilibration and eventual homogeneity of $Li^+$ vacancies lead to a continual reduction in diffusion *via* TSH, due to the dilution of divacancies, and eventual dominance of the ODH pathway. Upon review of similar muon experiments on isostructural materials (*e.g.* $LiCoO_2$, $LiCrO_2$ and $LiNiO_2$) a contribution at low $T$ may also be present, although much weaker in magnitude.[28,33] Previous studies have found that the inclusion of Al into $LiNi_{0.5}Co_{0.5}O_2$ increases the $Li^+$ diffusion coefficient of the host material.[46] We therefore suggest this increase occurs by promoting the more facile TSH mechanism, leading to the exaggerated contribution observed by μSR *versus* other materials.

The lithium diffusion coefficients ($D_{Li}$) for both TSH and ODH can be calculated with eqn (2), where $N_i$ is the number of accessible $Li^+$ sites in the $i^{th}$ path, $Z_{\nu,i}$ is the vacancy fraction of the destination sites, $s_i$ is the jump distance between $Li^+$ sites, and $\nu$ is the fluctuation rate at each temperature.[47] For ODH, $s_i$ is equal to the $a$ lattice parameter calculated from NPD (2.87 Å) and for TSH it is equal to $a \times \sqrt{3}$ (4.97 Å).

$$D_{Li} = \sum_{i=1}^{n} \frac{1}{N_i} Z_{\nu,i} s_i^2 \nu \quad (2)$$

The $D_{Li}^{ODH}$ and $D_{Li}^{TSH}$ were calculated to be $3 \times 10^{-11}$ and $3 \times 10^{-10}$ $cm^2\ s^{-1}$, respectively, for $Li_{0.87}NCA$, and $3 \times 10^{-11}$ and $2 \times 10^{-10}$ $cm^2\ s^{-1}$, respectively, for $Li_{0.71}NCA$ at 300 K. The values of $D_{Li}$ estimated from μSR agree with the values of $D_{Li}$ estimated using EIS and are further supported by first principles calculations.

Fig. 7(b) shows the Arrhenius plots for the muon hopping, giving rise to an $E_a^{ODH}$ of 90 ± 13 and 65 ± 6 meV and $E_a^{TSH}$ of 25 ± 1 and 21 ± 1 meV for $Li_{0.87}NCA$ and $Li_{0.71}NCA$, respectively.

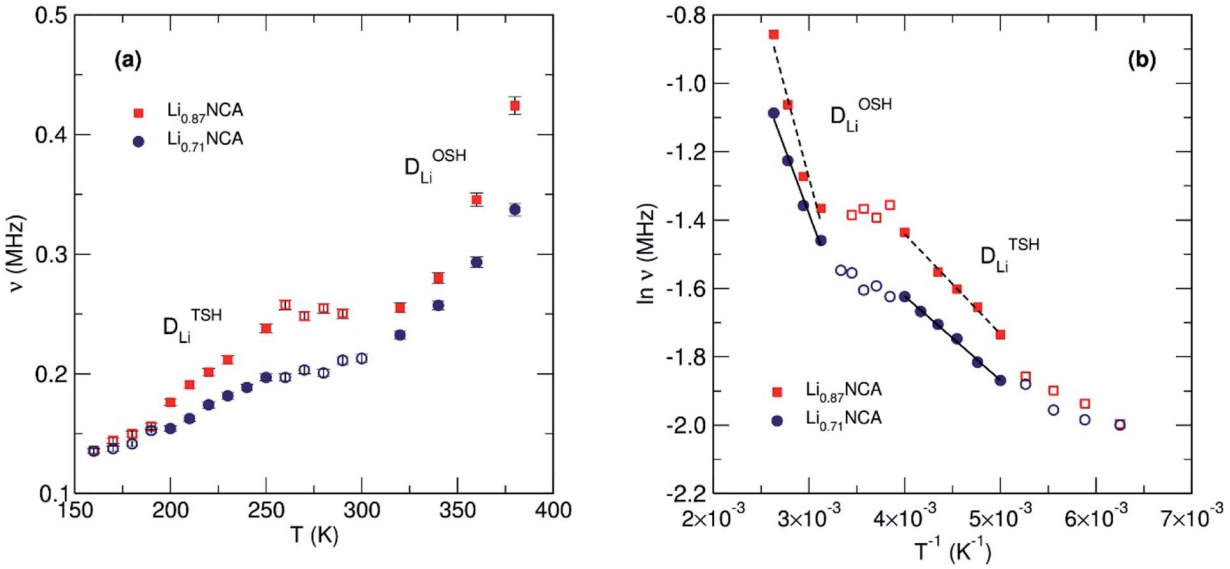


Fig. 7 (a) Fluctuation rate ($\nu$) *versus* temperature for $Li_{0.87}NCA$ and $Li_{0.71}NCA$ showing two responses from $Li^+$ diffusion and (b) Arrhenius plot of the fluctuation rate *versus* reciprocal temperature allowing calculation of $E_a$ and $D_{Li}$.

Table 3 Summary of calculated values for lithium diffusion coefficient ($D_{Li}$) at 300 K and activation energy of $Li^+$ diffusion ($E_a$) of lithium ion diffusion for $Li_{0.87}NCA$ and $Li_{0.71}NCA$

| | $D_{Li}$ ($cm^2\ s^{-1}$) | | $E_a$ (meV) | |
|---|---|---|---|---|
| Sample | EIS | μSR | DFT[24] | μSR |
| $Li_{0.87}NCA$ | $3 \times 10^{-11}$ | ODH: $3 \times 10^{-11}$<br>TSH: $3 \times 10^{-10}$ | ODH: $10^{-11}$ | ODH: $90 \pm 13$<br>TSH: $25 \pm 1$ |
| $Li_{0.71}NCA$ | $1 \times 10^{-11}$ | ODH: $3 \times 10^{-11}$<br>TSH: $2 \times 10^{-10}$ | TSH: $10^{-10}$ | ODH: $65 \pm 6$<br>TSH: $21 \pm 1$ |

We observe that the activation energies for both hopping mechanisms are lower in $Li_{0.71}NCA$, likely due to less Li–Li repulsion. The $E_a$ for TSH in both cases agrees well with values proposed for a divacancy mechanism in $LiCoO_2$ from PBE-SP calculations where values were as low as 15 meV.[48] The results obtained for the activation energies ($E_a$) for $Li^+$ diffusion for OSH and TSH were also close to previous computational studies, with respect to $E_a^{TSH} \approx \frac{1}{4} \times E_a^{OSH}$.

## Conclusions

For the first time experimental evidence has been provided for the presence of two distinct diffusion pathways (ODH and TSH) operating in a layered intercalation cathode, NCA. Potential local structure contributions to multiple observed diffusion pathways (such as cation mixing and impurity phases) were ruled out using PXRD and NPD, and possible magnetic effects eliminated by scrutiny of $\Delta$ by μSR.

Table 3 shows a summary of the values obtained from EIS and μSR. While both techniques are in good agreement with respect to estimated $D_{Li}$, bulk techniques have been unable to distinguish between individual diffusion pathways highlighting the use of μSR as a powerful tool to understand technologically important/relevant materials. These results obtained from μSR are also in good agreement with values obtained from first principles calculations on $LiCoO_2$.

It has also been experimentally demonstrated that the TSH mechanism requires a lower $E_a$ and operates at a faster rate compared to the ODH mechanism. This is of much importance to energy materials research, as manipulation of layered cathode materials' structures to promote divacancies will lead to more facile diffusion, and ultimately more efficient battery operation. These experiments suggest that this may be achieved by cationic substitution with elements that promote the TSH mechanism, such as Al.

## Experimental

### Preparation of lithium nickel cobalt aluminium oxide (NCA)

Samples of $Li_xNi_{0.8}Co_{0.15}Al_{0.05}O_2$ were prepared *via* solid-state based methods. All raw materials were purchased from Sigma Aldrich (Dorset, UK) unless stated otherwise. Solid state synthesis was carried out by placing 3.15 g (99.9%) of $Ni(NO_3)_2 \cdot 6H_2O$, 0.59 g (99.9%), of $Co(NO_3)_3 \cdot 6H_2O$, 0.25 g (99.9%) of $Al(NO_3)_3 \cdot 9H_2O$ and 0.97 g (99.9%) LiOH in to a glass beaker. 30 mL of isopropanol was added to the mixture and the resulting brown slurry was mixed using a high shear mixer (IKA Ultra-Turrax T25) for 5 min at 10 000 rpm to give a homogenous mixture. The mixture was transferred to a ceramic crucible and placed in a box furnace for 30 min at 75 °C to evaporate the isopropanol. The temperature was then ramped at 10 °C $min^{-1}$ to 850 °C and held for 5 h, yielding a black solid material. After heat treatment, potential LiOH or $Li_2O$ impurities were removed by washing with 0.05 M acetic acid (1 × 30 mL), water (3 × 30 mL) and isopropanol (1 × 30 mL) by centrifugation and dried in a vacuum oven overnight at 60 °C giving rise to sample $Li_{0.87}NCA$. $Li_{0.71}NCA$ was produced by using an identical methodology using 4 g of nanoparticle precursor (see ESI†) in place of the nitrate precursors.

 

### Physical characterisation

Powder X-ray Diffraction (PXRD) patterns were collected using a STOE Stadi P diffractometer (Mo $K\alpha_1$ radiation, $\lambda = 0.70932$ Å) in transmission geometry equipped with a germanium (111) monochromator and a DECTRIS Mythen 1K silicon strip detector (Dectris, Baden, Switzerland). An yttria ($Y_2O_3$) standard was used to estimate instrumental peak broadening. Datasets were collected over the $2\theta$ range of 2 to 40° with a step size of 0.5° and a count time of 20 s per step. Rietveld refinement was performed using the FullProf™ software package.[49] Neutron powder diffraction (NPD) was carried out on the iMATERIA diffractometer at J-PARC in Tokai, Japan.[50] The data was analysed by Rietveld refinement using the Z-Rietveld software package.[51,52]

Scanning Electron Microscopy (SEM) was performed using a JEOL JSM-6700F microscope. To minimise charging samples were deposited on copper foil tape, mounted on aluminium stubs, after dispersion in methanol (99.9%, Sigma Aldrich, Dorset, UK) and ultrasonication in a XUBA3 Ultrasonic Bath (Grant Instruments, Cambridge, UK) for 5 minutes. Image analysis was carried out using ImageJ software, calculating the average size over 200 particles for each sample.

X-ray fluorescence (XRF) spectroscopy was performed on the synthesised powders using an Epsilon 4 spectrometer (Malvern Panalytical, Malvern, UK). A nominal <2% total relative error applies to the observed values.

### Electrochemical characterisation

Electrodes were prepared by mixing of the active material ($Li_xNCA$) with binder (polyvinylidene fluoride, PVDF, PI-KEM, Staffordshire, UK) and conductive carbon black (Super P, Alfa Aesar, Heysham, UK) in a ratio of 80 : 10 : 10 wt%. A 10 wt% solution of PVDF in *N*-methyl-2-pyrrolidone, NMP (Sigma Aldrich, Dorset, UK) was prepared using a magnetic stirrer and then mixed by hand with the conductive carbon and the active material. Further NMP (2.5 mL) was added to give a viscous slurry. The slurry was ball-milled at 800 rpm for 1 h before being cast on 15 μm thick aluminium foil (PI-KEM, Staffordshire, UK). The electrode sheets were dried on a hotplate at *ca.* 150 °C for 20 min.

All half-cell testing of the NCA materials were performed in CR2032 coin cells at room temperature on a Gamry Instruments Interface 1000 Galvanostat/Potentiostat (SciMed, Cheshire, UK). All cells were assembled in an Ar-filled glovebox with $O_2$ and $H_2O$ < 0.5 ppm. GF/B glass microfiber filters (Whatman, Buckinghamshire, UK) were used as separators and drenched in electrolyte of 1 M $LiPF_6$ in 1 : 1 wt% ethylene carbonate/diethyl methyl carbonate (BASF, Ludwigshafen, Germany). Lithium metal foil 15.6 mm diameter, 0.45 mm thick (PI-KEM, Staffordshire, UK) was used as a counter electrode. Potentiostatic EIS was carried out from 1 to $10^6$ Hz at 10 mV AC RMS and 0 V DC *versus* open circuit voltage.

### Muon spin relaxation (μSR)

Muon spin relaxation experiments were performed at STFC ISIS Neutron and Muon Source, Didcot, UK. Approximately 3 g of powdered samples of $Li_{0.87}NCA$ and $Li_{0.71}NCA$ were packed into recessed titanium samples holders, covered with a titanium window and secured with a titanium bezel. The titanium holder provides a simple background signal from muons which are not implanted into the sample and is easily subtracted from the data. The sample holder was placed into the muon spectrometer (EMU) and evacuated to $<1 \times 10^{-6}$ mbar. The instrument was cooled to a temperature of 160 K and the instrument asymmetry was measured using a transverse magnetic field of 20 G. Measurements were taken every 10 K up to 380 K with longitudinal at fields of 0, 5 and 10 G. Data collected at each temperature for the three applied magnetic fields were fit simultaneously using the WiMDA software.[53]

## Conflicts of interest

There are no conflicts to declare.

## Note added after first publication

This article replaces the version published on 28th May 2020, which contained errors in the Fig. 4 and Fig. 5 captions.

## Acknowledgements

Muon experiments at the ISIS Neutron and Muon Source were supported by beamtime allocation RB1810738 from the Science and Technology Facilities Council.[54] Neutron experiments at the J-PARC Materials & Life Science Division were supported by beamtime allocation 2018B0196. JAD, ARG and TEA would like to thank the EPSRC grant EP/R023662/1, Joint University Industry Consortium for Energy (Materials) and Devices Hub (JUICED), for support.

## References

1 UNFCCC, *Conference of the Parties (COP), Paris Clim. Chang. Conf. - Novemb. 2015, COP 21*, FCCC/CP/2015/L.9/Rev.1.
2 H. S. Baker, R. J. Millar, D. J. Karoly, U. Beyerle, B. P. Guillod, D. Mitchell, H. Shiogama, S. Sparrow, T. Woollings and M. R. Allen, *Nat. Clim. Change*, 2018, **8**, 604–608.
3 J.-M. Tarascon, *Philos. Trans. R. Soc., A*, 2010, **368**, 3227–3241.
4 K. Mizushima, P. C. Jones, P. J. Wiseman and J. B. Goodenough, *Mater. Res. Bull.*, 1980, **15**, 783–789.
5 N. Nitta, F. Wu, J. T. Lee and G. Yushin, *Mater. Today*, 2015, **18**, 252–264.
6 A. Rougier, P. Gravereau and C. Delmas, *J. Electrochem. Soc.*, 1996, **143**, 1168.
7 T. Ohzuku, A. Ueda, M. Nagayama, Y. Iwakoshi and H. Komori, *Electrochim. Acta*, 1993, **38**, 1159–1167.
8 C. Vogler, B. Löffler, W. Weirather, M. Wohlfahrt-Mehrens and J. Garche, *Ionics*, 2002, **8**, 92–99.
9 J. Dahn, E. Fuller, M. Obrovac and U. Vonsacken, *Solid State Ionics*, 1994, **69**, 265–270.
10 T. Ohzuku, *J. Electrochem. Soc.*, 1995, **142**, 4033.
11 H. Arai and Y. Sakurai, *J. Power Sources*, 1999, **81–82**, 401–405.

12 S. Albrecht, J. Kümpers, M. Kruft, S. Malcus, C. Vogler, M. Wahl and M. Wohlfahrt-Mehrens, *J. Power Sources*, 2003, **119–121**, 178–183.
13 C. H. Chen, J. Liu, M. E. Stoll, G. Henriksen, D. R. Vissers and K. Amine, *J. Power Sources*, 2004, **128**, 278–285.
14 R. Kostecki, J. Lei, F. McLarnon, J. Shim and K. Striebel, *J. Electrochem. Soc.*, 2006, **153**, A669.
15 R. S. Nicholson and I. Shain, *Anal. Chem.*, 1964, **36**, 706–723.
16 H. Xia, L. Lu and G. Ceder, *J. Power Sources*, 2006, **159**, 1422–1427.
17 P. P. Prosini, M. Lisi, D. Zane and M. Pasquali, *Solid State Ionics*, 2002, **148**, 45–51.
18 W. Weppner, *J. Electrochem. Soc.*, 1977, **124**, 1569.
19 R. Amin, D. B. Ravnsbaek and Y.-M. Chiang, *J. Electrochem. Soc.*, 2015, **162**, A1163–A1169.
20 F. Qi, C. Rier, R. Böhmer, W. Franke and P. Heitjans, *Phys. Rev. B: Condens. Matter Mater. Phys.*, 2005, **72**, 104301.
21 T. E. Ashton, J. V. Laveda, D. A. MacLaren, P. J. Baker, A. Porch, M. O. Jones and S. A. Corr, *J. Mater. Chem. A*, 2014, **2**, 6238–6245.
22 M. Amores, T. E. Ashton, P. J. Baker, E. J. Cussen and S. A. Corr, *J. Mater. Chem. A*, 2016, **4**, 1729–1736.
23 I. D. Johnson, T. E. Ashton, E. Blagovidova, G. J. Smales, M. Lübke, P. J. Baker, S. A. Corr and J. A. Darr, *Sci. Rep.*, 2018, **8**, 4114.
24 A. Van der Ven, *Electrochem. Solid-State Lett.*, 1999, **3**, 301.
25 D. A. Tompsett and M. S. Islam, *Chem. Mater.*, 2013, **25**, 2515–2526.
26 A. Urban, D.-H. Seo and G. Ceder, *npj Comput. Mater.*, 2016, **2**, 16002.
27 J. Sugiyama, H. Nozaki, M. Harada, K. Kamazawa, O. Ofer, M. Månsson, J. H. Brewer, E. J. Ansaldo, K. H. Chow, Y. Ikedo, Y. Miyake, K. Ohishi, I. Watanabe, G. Kobayashi and R. Kanno, *Phys. Rev. B: Condens. Matter Mater. Phys.*, 2011, **84**, 054430.
28 J. Sugiyama, Y. Ikedo, K. Mukai, H. Nozaki, M. Månsson, O. Ofer, M. Harada, K. Kamazawa, Y. Miyake, J. H. Brewer, E. J. Ansaldo, K. H. Chow, I. Watanabe and T. Ohzuku, *Phys. Rev. B: Condens. Matter Mater. Phys.*, 2010, **82**, 224412.
29 J. Sugiyama, K. Mukai, Y. Ikedo, H. Nozaki, M. Månsson and I. Watanabe, *Phys. Rev. Lett.*, 2009, **103**, 147601.
30 J. Sugiyama, Y. Ikedo, K. Mukai, H. Nozaki, M. Månsson, O. Ofer, M. Harada, K. Kamazawa, Y. Miyake, J. H. Brewer, E. J. Ansaldo, K. H. Chow, I. Watanabe and T. Ohzuku, *Phys. Rev. B: Condens. Matter Mater. Phys.*, 2010, **82**, 224412.
31 J. Sugiyama, H. Nozaki, M. Harada, K. Kamazawa, Y. Ikedo, Y. Miyake, O. Ofer, M. Månsson, E. J. Ansaldo, K. H. Chow, G. Kobayashi and R. Kanno, *Phys. Rev. B: Condens. Matter Mater. Phys.*, 2012, **85**, 054111.
32 J. Sugiyama, K. Mukai, M. Harada, H. Nozaki, K. Miwa, T. Shiotsuki, Y. Shindo, S. R. Giblin and J. S. Lord, *Phys. Chem. Chem. Phys.*, 2013, **15**, 10402.
33 M. Månsson, H. Nozaki, J. M. Wikberg, K. Prša, Y. Sassa, M. Dahbi, K. Kamazawa, K. Sedlak, I. Watanabe and J. Sugiyama, *J. Phys.: Conf. Ser.*, 2014, **551**, 012037.
34 M. A. Cabañero, N. Boaretto, M. Röder, J. Müller, J. Kallo and A. Latz, *J. Electrochem. Soc.*, 2018, **165**, A847–A855.
35 M. Dixit, M. Kosa, O. S. Lavi, B. Markovsky, D. Aurbach and D. T. Major, *Phys. Chem. Chem. Phys.*, 2016, **18**, 6799–6812.
36 S. P. Ong, V. L. Chevrier, G. Hautier, A. Jain, C. Moore, S. Kim, X. Ma and G. Ceder, *Energy Environ. Sci.*, 2011, **4**, 3680.
37 N. M. Trease, I. D. Seymour, M. D. Radin, H. Liu, H. Liu, S. Hy, N. Chernova, P. Parikh, A. Devaraj, K. M. Wiaderek, P. J. Chupas, K. W. Chapman, M. S. Whittingham, Y. S. Meng, A. Van der Van and C. P. Grey, *Chem. Mater.*, 2016, **28**, 8170–8180.
38 L. de Biasi, A. O. Kondrakov, H. Geßwein, T. Brezesinski, P. Hartmann and J. Janek, *J. Phys. Chem. C*, 2017, **121**, 26163–26171.
39 R. Koerver, W. Zhang, L. de Biasi, S. Schweidler, A. O. Kondrakov, S. Kolling, T. Brezesinski, P. Hartmann, W. G. Zeier and J. Janek, *Energy Environ. Sci.*, 2018, **11**, 2142–2158.
40 A. O. Kondrakov, A. Schmidt, J. Xu, H. Geßwein, R. Mönig, P. Hartmann, H. Sommer, T. Brezesinski and J. Janek, *J. Phys. Chem. C*, 2017, **121**, 3286–3294.
41 R. Robert and P. Novak, *J. Electrochem. Soc.*, 2015, **162**, A1823–A1828.
42 A. J. Bard and L. R. Faulkner, *Electrochemical Methods: Fundamentals and Applications*, John Wiley & Sons, Inc., 2nd edn, 2001.
43 M. Itagaki, N. Kobari, S. Yotsuda, K. Watanabe, S. Kinoshita and M. Ue, *J. Power Sources*, 2005, **148**, 78–84.
44 A. Matasso, D. Wong, D. Wetz and F. Liu, *J. Electrochem. Soc.*, 2015, **162**, A885–A891.
45 R. S. Hayano, Y. J. Uemura, J. Imazato, N. Nishida, T. Yamazaki and R. Kubo, *Phys. Rev. B: Condens. Matter Mater. Phys.*, 1979, **20**, 850–859.
46 S. Castro-García, A. Castro-Couceiro, M. A. Señarís-Rodríguez, F. Soulette and C. Julien, *Solid State Ionics*, 2003, **156**(1–2), 15–26.
47 R. Borg and G. Dienes, *An introduction to solid state diffusion*, Elsevier, Burlington, MA, 1st edn, 2012.
48 A. Moradabadi and P. Kaghazchi, *Phys. Chem. Chem. Phys.*, 2015, **17**, 22917–22922.
49 J. Rodríguez-Carvajal, *Phys. B*, 1993, **192**, 55–69.
50 T. Ishigaki, A. Hoshikawa, M. Yonemura, T. Morishima, T. Kamiyama, R. Oishi, K. Aizawa, T. Sakuma, Y. Tomota, M. Arai, M. Hayashi, K. Ebata, Y. Takano, K. Komatsuzaki, H. Asano, Y. Takano and T. Kasao, *Nucl. Instrum. Methods Phys. Res., Sect. A*, 2009, **600**(1), 89–191.
51 R. Oishi, M. Yonemura, Y. Nishimaki, S. Torii, A. Hoshikawa, T. Ishigaki, T. Morishima, K. Mori and T. Kamiyama, *Nucl. Instrum. Methods Phys. Res., Sect. A*, 2009, **600**(1), 94–96.
52 R. Oishi-Tomiyasu, M. Yonemura, T. Morishima, A. Hoshikawa, S. Torii, T. Ishigaki and T. Kamiyama, *J. Appl. Crystallogr.*, 2012, **45**, 299–308.
53 F. L. Pratt, *Phys. B*, 2000, **289–290**, 710–714.
54 T. E. Ashton, J. A. Darr and P. J. Baker, *STFC ISIS Neutron Muon Source*, DOI: 10.5286/ISIS.E.RB1810738.

 